Accepted Manuscript

Design of balanced COX inhibitors based on anti-inflammatory and/or COX-2 inhibitory ascidian metabolites

Zhiran Ju, Mingzhi Su, Jongki Hong, Eun La Kim, Hyung Ryong Moon, Hae Young Chung, Suhkmann Kim, Jee H. Jung

PII: S0223-5234(19)30637-3

DOI: https://doi.org/10.1016/j.ejmech.2019.07.016

Reference: EJMECH 11513

To appear in: *European Journal of Medicinal Chemistry*

Received Date: 24 May 2019

Revised Date: 5 July 2019

Accepted Date: 5 July 2019

Please cite this article as: Z. Ju, M. Su, J. Hong, E. La Kim, H.R. Moon, H.Y. Chung, S. Kim, J.H. Jung, Design of balanced COX inhibitors based on anti-inflammatory and/or COX-2 inhibitory ascidian metabolites, *European Journal of Medicinal Chemistry* (2019), doi: https://doi.org/10.1016/j.ejmech.2019.07.016.

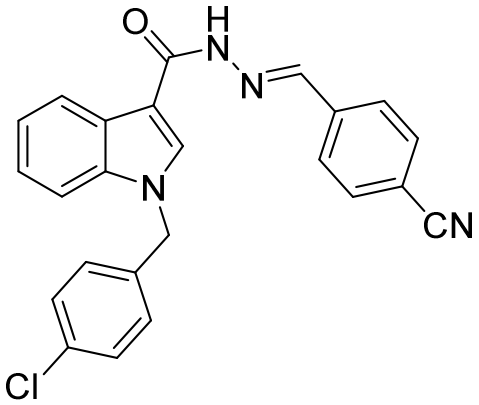

5m

balanced COX-1/COX-2 inhibitor

A

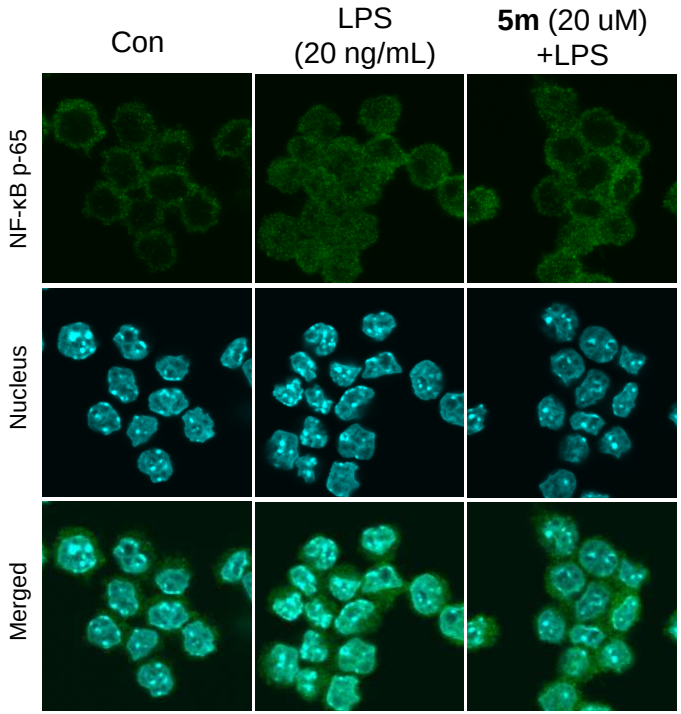

Design of balanced COX inhibitors based on anti-inflammatory and/or COX-2 inhibitory ascidian metabolites

Zhiran Ju [a,†], Mingzhi Su [a,†], Jongki Hong [b], Eun La Kim [a], Hyung Ryong Moon [a], Hae Young Chung [a], Suhkmann Kim [c], Jee H. Jung [a,*]

[a] College of Pharmacy, Pusan National University, Busan 46241, Republic of Korea

[b] College of Pharmacy, Kyunghee University, Seoul 02447, Republic of Korea

[c] Center for Proteome Biophysics, Department of Chemistry, Pusan National University, Busan 46241, Republic of Korea

*Correspondence: jhjung@pusan.ac.kr (J.H.J.); +82-51-510-2803 (J.H.J.).
[†]These authors equally contributed to this work

Abstract: The aim of this study was to design and synthesize COX-1/COX-2 balanced inhibitors incorporating the structural motifs of anti-inflammatory ascidian metabolites. We designed a series of substituted indole analogs that incorporate the key structures of the ascidian metabolites, herdmanines C and D. The synthesized analogs were tested for their inhibitory activity against COX-1 and COX-2, and compound **5m**, which displayed balanced inhibition, was further evaluated for in vitro anti-inflammatory activity. Compound **5m** suppressed the expression of pro-inflammatory factors, including iNOS, COX-2, TNF-α, and IL-6 in LPS-stimulated murine RAW264.7 macrophages. The reduction of PGE_2, NO, and ROS was also observed, together with the suppression of NF-κB, IKK, and IκBα phosphorylation. Our results characterized **5m** as a COX-1/COX-2 balanced inhibitor that subsequently caused ROS inhibition and NF-κB suppression, and culminated in the suppression of iNOS, COX-2, TNF-α, and IL-6 expression.

Keywords: COX-1/COX-2, balanced inhibition, anti-inflammatory, NF-κB pathway, indole, ascidian metabolite

1. Introduction

Although non-steroidal anti-inflammatory drugs (NSAIDs) are the most frequent choice of treatment for inflammatory symptoms, they are often accompanied by undesirable side effects on the renal, hepatic, and cardiovascular systems [1]. Therefore, the discovery of new NSAIDs with better safety profiles remains a major challenge. Generally, two different strategies are employed for the development of new NSAIDs. The first is the development of inhibitors of the production of prostaglandin (PG) E_2 and arachidonic acid metabolites, which are potent mediators of inflammation. Cyclooxygenases (COX-1 and -2) are essential for the biosynthesis of these mediators [1,2,9]. The other is the development of inhibitors of iNOS (inducible nitric oxide synthase). iNOS contributes to acute and chronic inflammation through the production of nitric oxide as a cytotoxic inflammatory mediator [3-4]. Traditional NSAIDs exhibit pharmacological action through the inhibition of cyclooxygenase (COX) activity in vivo and the reduction of the biosynthesis of prostaglandins in local tissues. At present, it is believed that NSAID inhibitory effects of COX is the basis of their pharmacodynamic effect. Therefore, COX proteins are recognized as indispensable targets for drug development [1,5-7]. Two isoforms of COX, with distinct physiological roles, are well defined. COX-1, which is constitutively expressed in various tissues, is described as a housekeeping enzyme that regulates normal cellular processes, such as gastric cytoprotection, vascular homeostasis, platelet aggregation, and kidney function [7]. In contrast, COX-2 remains at very low levels in most tissues and is only rapidly upregulated during states of inflammation, in which it causes the elevated production of prostanoids that occurs at sites of disease and inflammation [5-7].

Traditional non-selective COX inhibitors, such as aspirin, phenazone, and indomethacin, are effective for the treatment of inflammatory diseases, but are also associated with major drawbacks through the decrease in the cytoprotective action of the constitutive COX-1 isoform in the gastrointestinal tract leading to ulcerogenic, hepatic, and renal toxicity [7-9]. Therefore, COX-2 selective inhibitors, such as celecoxib, rofecoxib, and valdecoxib, were developed as anti-inflammatory agents with reduced gastrointestinal side effects. However, these COX-2 selective inhibitors were found to be associated with other side effects, such as

cardiovascular disorders due to imbalance in the COX pathway [9-11]. These undesirable side effects often resulted in their withdrawal from the market. Recently, Wallace et al. indicated that the inhibition of COX-1 led to the upregulation of COX-2, which may counteract the deleterious effects caused by COX-1 inhibition, such as gastric hypermobility and the subsequent events caused by PG deficiency [7,8]. Furthermore, the inhibition of COX-1 significantly contributes to the resolution of inflammation [12]. In the process of ulcer healing, COX-1 specific inhibitors, as well as COX-2 specific inhibitors, delay healing [12]. These findings proved that although COX-2 indeed plays a pivotal role in the inflammatory process, COX-1/COX-2 balanced inhibitors appear more favorable, in some respects, when the critical side effects of either non-selective or selective inhibitors are considered [13-15].

Herein, motivated by the anti-inflammatory ascidian metabolites, herdmanines (Fig. 1), we designed and synthesized two series of indole derivatives of balanced inhibitory activity to COX-1 and COX-2, with the expectation of producing effective anti-inflammatory agents with an improved safety profile.

2. Design strategy for COX inhibitors based on natural anti-inflammatory compounds and clinically used NSAIDs

In our previous work, new anti-inflammatory amino acid derivatives herdmanines C and D were isolated from the ascidian *Herdmania momus* [16,17]. Herdmanines C and D showed moderate suppressive effects on COX-2, iNOS, IL-6, and NO production [16]. Therefore, herdmanines C and D were examined *in silico* for COX LBD (ligand binding domain) binding by docking simulation, and they showed fair affinity to the ligand binding domain of COX-1 and 2 (see SI). The guanidyl moiety of herdmanine C and the carboxyl moiety of herdmanine D showed similar hydrogen bondings as the carboxyl moiety of indomethacin. The carboxyl group of indomethacin works as a hydrogen bond donor and forms H bonds with Arg^{120} and Tyr^{355} of COX-2 LBD (Fig. 8B). The 2-imino-4-thiazolidinone moiety of darbufelone also behaved as a polar head and formed hydrogen bondings with the LBD of COX. Classical COX inhibitors like indomethacin and darbufelone are composed of polar head and

hydrophobic tail. Therefore, the target molecules were designed to contain the acylhydrazone moiety which may work as hydrogen bond donor as isosteres of guanidyl moiety of herdmanine C, the carboxyl group of indomethacin, and the 2-imino-4-thiazolidinone moiety of darbufelone. The acylhydrazone moiety is widely used as pharmacophore block for the synthesis of a variety of novel bioactive compounds, and many hydrazone derivatives have been claimed to possess anti-inflammatory activity, including COX inhibitory activity [20-24]. In addition to the acylhydrazone moiety, the target scaffold includes indole moiety and halobenzyl or halobenzoyl moieties, in part to mimic the partial structures of herdmanine D and indomethacin, and also to facilitate hydrophobic interactions with the ligand binding domain of COX. The halobenzyl or halobenzoyl moieties are important for binding to the COX active site, and for stabilization of the hydrophobic interactions with the key amino acids in COX [25]. Therefore, synthetic derivatives were designed to incorporate acylhydrazone, indole, and halobenzyl/halobenzoyl moieties (Fig. 1).

Based on our original design, a hydrogen bond donor acylhydrazone moiety was placed at the C-3 position of the indole and the physicochemical properties of the alkyl and aryl groups were varied (**4a**–**4u**, Scheme 1). A chlorobenzyl moiety was introduced in **5a**–**5u** and the halobenzoyl moieties were introduced in **6a**/**6b** at the *N*-1 position of indole.

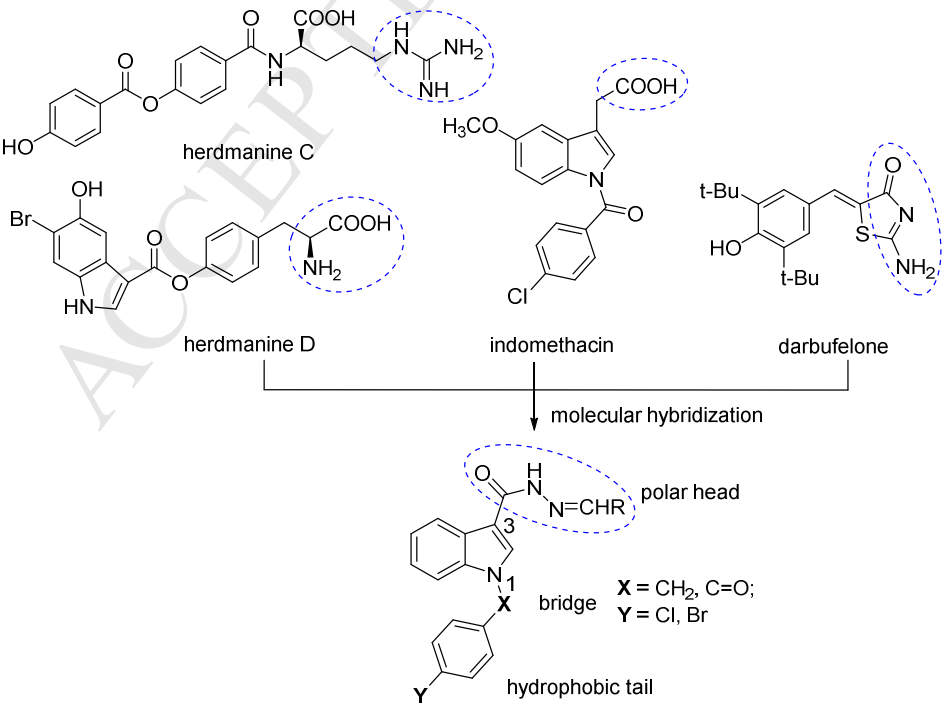

Fig. 1. Design of COX inhibitors incorporating the partial structures of herdmanines and traditional NSAIDs. Dotted circles show tentative hydrogen bond donors.

3. Results and Discussion

3.1. Chemistry

The synthesis of the target compounds is depicted in Scheme 1. Starting from indole-3-carboxylic acid (**1**), a methyl ester (**2**) was prepared (77%) by the esterification reaction (90°C) with anhydrous methyl alcohol in the presence of a few drops of dilute sulfuric acid. The 1*H*-indole-3-carbohydrazide (**3**) was prepared with a 96% yield by the hydrazinolysis of **2** with 98% hydrazine hydrate in absolute ethanol. The indole *N*-arylhydrazone derivatives (**4a**–**4u**) were synthesized by the condensation of **3** with various substituted aldehydes in the presence of ethanol and a few drops of propionic acid [26], and the reaction was straightforward in most of the cases. The resulting indole *N*-arylhydrazone derivatives (**4a**–**4u**) were employed as starting compounds for the synthesis of indolyl-*N*-substituted benzyl/benzoyl derivatives. The target compounds, indolyl-*N*-substituted benzyl/benzoyl derivatives (**5a**–**5u** and **6a**–**6b**), were prepared by the reaction of **4a**–**4u** with benzyl chloride and benzoyl chloride/bromide in the presence of NaH in DMF at room temperature for 24 h [9]. The final products were characterized by ^{1}H-NMR, ^{13}C-NMR, and mass spectrometric analysis.

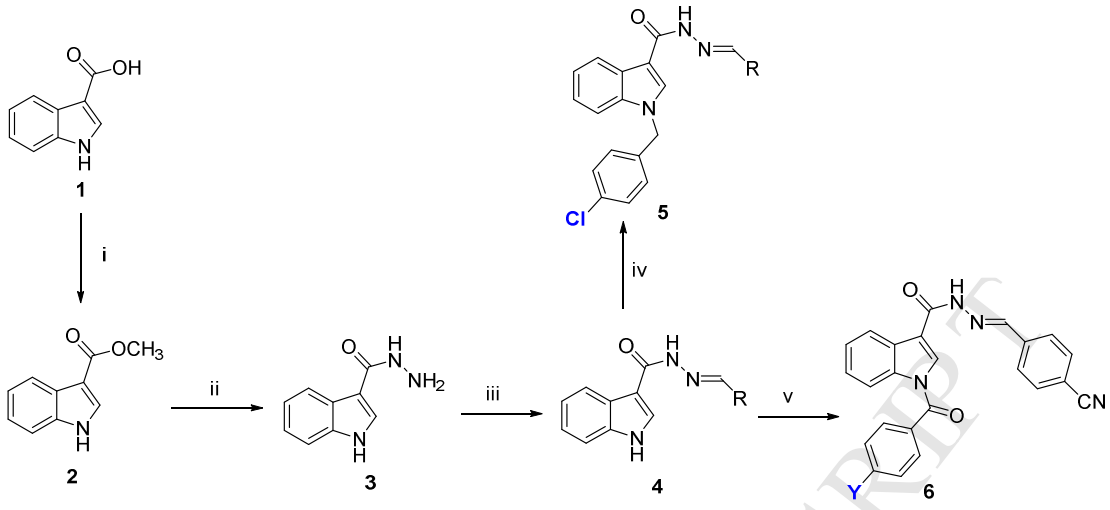

5a R = $CH(CH_3)_2$
5b R = $C(CH_3)_3$
5c R = 2-methylbutyl
5d R = cyclopropyl
5e R = cyclohexyl
5f R = $(CH_2)_4CH_3$
5g R = $(CH_2)_7CH_3$
5h R = CH_2CH_2Ph
5i R = Ph
5j R = Ph-4-OH
5k R = Ph-4-Cl
5l R = Ph-4-OCH_3
5m R = Ph-4-CN
5n R = Ph-4-Br
5o R = Ph-4-COOH
5p R = Ph-4-F
5q R = Ph-3,5-dichloro
5r R = Ph-3,5-dibromo
5s R = Ph-3-chloro-5-OCH_3
5t R = 4-methylthiazol-5-yl
5u R = 2-furyl

6a Y= Cl
6b Y= Br

Scheme 1. Reagents and conditions: (i) dilute H_2SO_4, MeOH, reflux, 24 h; (ii) NH_2-NH_2.H_2O, EtOH, reflux, 2 h; (iii) RCHO/EtOH, propionic acid, reflux, 2.5 h; (iv) 4-Cl-PhCH_2Cl, NaH, DMF, R.T., 24 h; (v) 4-Cl-PhCOCl/4-Br-PhCOCl, NaH, DMF, R.T., 24 h.

The geometry of the carbon-nitrogen double bond in **5a**–**5u** and **6a**–**6b** was determined as (*E*) through the comparison of ^{1}H NMR data with those reported for *N*-acylhydrazone derivatives [27, 28]. The chemical shift of the H-C=N hydrogen of **5a**–**5h** (δ_H 7.49–7.55), **5i**–**5u** and **6a**–**6b** (δ_H 8.22–8.37) was almost identical to those of *N*-acylhydrazone derivatives [27, 28] with (***E***) geometry. The sterically stable *E*-isomer predominated over the sterically hindered *Z*-isomer [29].

3.2. Biological evaluations

3.2.1. Evaluation of COX-1 and COX-2 inhibitory activities

The synthesized compounds (**5a**–**5u** and **6a**–**6b**) were tested for their ability to inhibit COX-1 and COX-2 by using an enzyme immunoassay (EIA). Of the tested compounds, the

cyanophenyl derivative **5m** showed substantial COX-1 and COX-2 inhibitory activities, with IC_{50} values of 39.20 and 7.59 μM, respectively (Fig. 2, Table 1). Compounds **5f** and **5u** also showed better activity than other analogs, and this result may be expected from the docking simulation (see SI). Of the branched alkyl, linear alkyl, and cycloalkyl derivatives, linear alkyl derivative (**5f**) appears a better option. However, substantially long alkyl chain (**5g**) would not be preferable. According to docking simulation, the COX-1 and COX-2 binding affinities of **5m**, **5f**, and **5u** were no less than others though the difference was not notable. Compounds **6a** and **6b** showed diminished activity than **5m** even though they share similar skeleton with **5m** except the *N*-benzyl/benzoyl substructure. This may be due to lower binding affinities of **6a** and **6b** than that of **5m** (see SI). The distinctively lower inhibitory activities of similar phenyl substituted analogs (**5j - 5s**) compared to that of **5m** would also be attributed to lower binding affinities of **5j - 5s**.

The COX-1 inhibitory activity of **5m** was milder than the tested NSAIDs (Table 1). Whilst, the COX-2 inhibitory activity of **5m** significantly potent (IC_{50} = 7.59 μM) and it was comparable with those of the tested NSAIDs. The COX inhibitory potency and COX-2 selectivity index (IC_{50} (COX-1)/IC_{50} (COX-2) of **5m** were compared with COX-2 selective (celecoxib and Dup-697), COX-1 selective (SC-560), and commercial non-selective drugs (Table 1). The COX-2 selectivity of **5m** was higher than ibuprofen, aspirin, and mesalazine, but it was much lower than that of celecoxib and Dup-697. The COX-2 selectivity of **5m** was similar to that of diclofenac. Notably, diclofenac is a widely used drug in inflammatory diseases, but has been associated with only mild GI side effects in both clinical trials and epidemiological studies [30-32]. In addition, diclofenac is devoid of cardiovascular side effects that are characteristic of COX-2 selective inhibitors such as celecoxib. These results suggested that the balanced COX-2 selectivity of **5m** may be favorable for development of NSAIDs with attenuated gastrointestinal and cardiovascular side effects. Subsequently, the in vitro anti-inflammatory activity of **5m** was examined at the cellular level by using RAW264.7 murine macrophages.

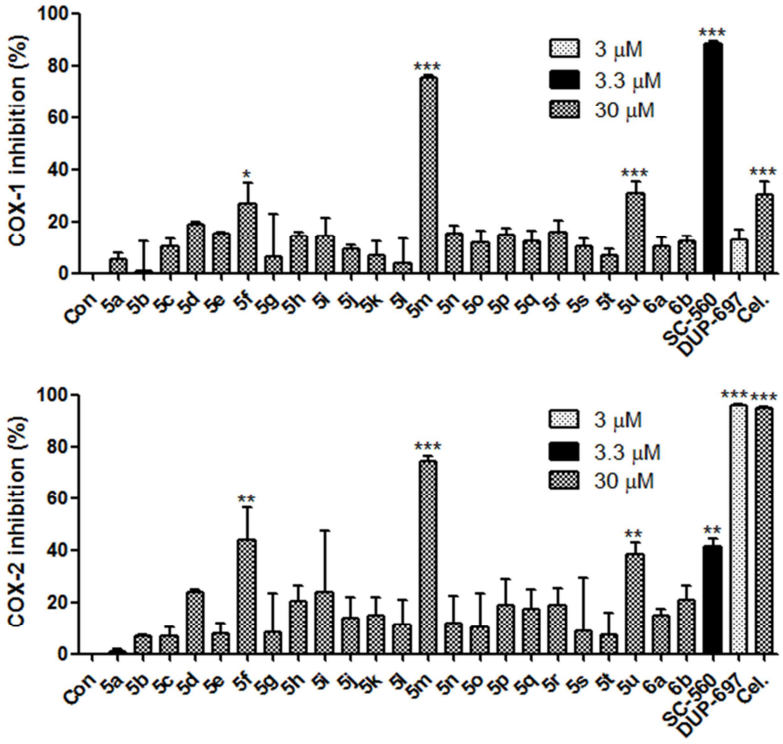

Fig. 2. *In-vitro* COX-1 and COX-2 enzyme inhibition assay of compounds **5a**–**5u** and **6a**–**6b**. SC-560 is a COX-1 selective inhibitor; DUP-697 and celecoxib (Cel.) are COX-2 selective inhibitors; Con: control (DMSO). The results are shown as the mean ± SD (n=3) of three independent experiments. $^{*}p < 0.05$, $^{**}p < 0.01$, $^{***}p < 0.001$ compared with the control group.

Table 1. *In vitro* COX-1/COX-2 inhibition (IC_{50}, μM) and selectivity index for compound **5m** and standard agents.

comp	COX-1[a]	COX-2[a]	COX-2 selectivity[b]
5m	39.20	7.59	5.16
SC-560	0.01	>3.30	<0.003
ibuprofen	4.12	8.91	0.46
aspirin	6.12	12.36	0.49
mesalazine	7.73	7.53	1.02
diclofenac	18.79	1.24	15.18
celecoxib	>100.00	1.31	>76.39
Dup-697	>3.00	0.02	>139.53

Note. [a]: The result (IC_{50}, μM) is the mean of three determinations acquired using a COX fluorescent

inhibitor screening assay kit (Cayman Chemical, MI, USA). [b]: COX-2 selectivity index (COX-1 IC_{50}/COX-2 IC_{50}). Celecoxib and DUP-697 were employed as selective COX-2 inhibitors, and SC-560 was employed as a COX-1 inhibitor.

3.2.2. Determination of in vitro cytotoxicity

Prior to the cell-based anti-inflammatory assay, compound **5m** was evaluated for its toxicity to murine macrophages (RAW264.7), rat liver cells (Ac2F), and mouse fibroblast cells (L929) to determine a suitable concentration for the anti-inflammatory assay. Compound **5m** was almost non-toxic to all of these cell lines at concentrations of up to 50 μM for 24 h. Therefore, murine macrophage cells (RAW264.7) were treated with **5m** at concentrations below 20 μM and subjected to an anti-inflammatory assay.

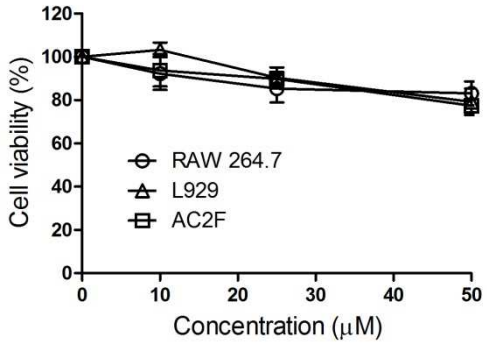

Fig. 3. Determination of the toxicity of **5m** (10, 25, and 50 μM) to RAW264.7 murine macrophages, the mouse fibroblast cell line L929, and rat liver Ac2F cells after exposure for 24 h.

*3.2.3. Compound **5m** inhibited LPS-induced expression of pro-inflammatory cytokines in RAW264.7 cells*

To gauge the in vitro anti-inflammatory effect of compound **5m**, the protein expression of the pro-inflammatory factors iNOS and COX-2 was examined by Western blotting. As expected, LPS stimulation markedly increased iNOS and COX-2 protein expression, but this increase was significantly and concentration-dependently downregulated by pretreatment of cells with **5m** (Fig. 4). Notably, compound **5m** (20 μM) attenuated the protein expression of both iNOS and COX-2 more potently than dexamethasone (10 μM).

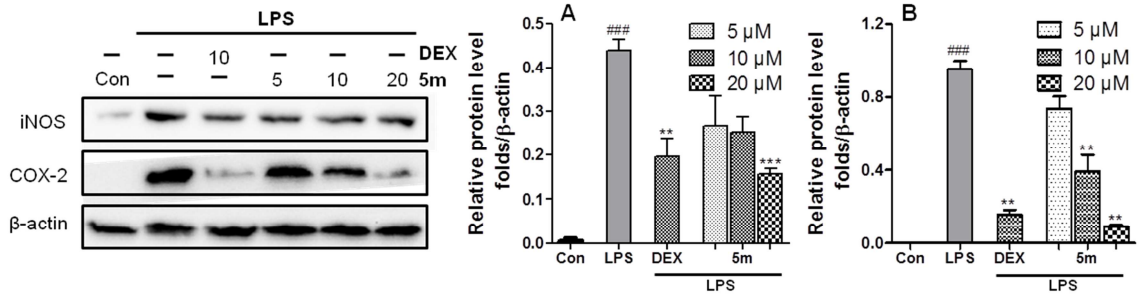

Fig. 4. Effects of **5m** on LPS-induced iNOS (**A**) and COX-2 (**B**) protein expression in RAW264.7 cells. The cells were treated with different concentrations of **5m**, and then cultured in the presence or absence of LPS (1 μg/mL) for 24 h. Dexamethasone (DEX) was employed as the positive control (10 μM). The results were shown as the mean ± SD (n=3) of three independent experiments. $^{###}p < 0.001$ compared with the control group; $^{**}p < 0.01$, $^{***}p < 0.001$ compared with the LPS-stimulated group.

During inflammation, pro-inflammatory stimuli induce the production of various cytokines and inflammatory mediators, such as nitric oxide (NO), prostaglandin E_2 (PGE_2), tumor necrosis factor α (TNF-α), and interleukin-6 (IL-6). As compound **5m** inhibited iNOS expression, it would, therefore, decrease NO production in macrophages. The amount of NO in RAW264.7 cell supernatants was measured using Griess reagent. As shown in Figure 5A, the NO production decreased in a concentration-dependent manner by compound **5m**. As an inflammatory mediator, a high production of PGE_2 will result from inflammatory stimuli. As COX-2 is a metabolic enzyme of PGE_2, the inhibition of COX-2 leads to a decrease in the production of PGE_2, as shown in Figure 5D.

In addition, the production of TNF-α and IL-6 was determined by enzyme-linked immunosorbent assay (ELISA). TNF-α and IL-6, which the inflammatory cytokines, are part of the host response to inflammatory situations and maintain normal cellular conditions [33]. As shown in Figures 5B and 5C, the amount of pro-inflammatory mediators was markedly increased when RAW264.7 murine macrophages were exposed to LPS, but this increase was prevented by **5m** in a dose-dependent manner. These results indicated that **5m** clearly attenuated an excessive immune reaction in LPS-stimulated RAW264.7 cells.

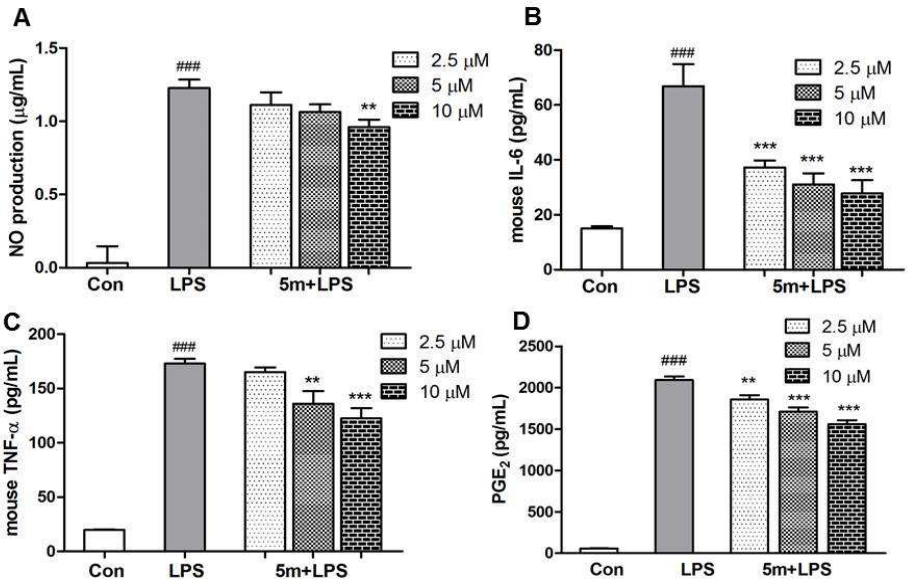

Fig. 5. Effects of compound **5m** on the production of (**A**) nitric oxide (NO), (**B**) interleukin-6 (IL-6), (**C**) tumor necrosis factor α (TNF-α), and (**D**) prostaglandin E_2 (PGE_2) in LPS-induced RAW264.7 macrophages. The cells were pretreated with different concentrations of **5m** (2.5, 5, or 10 μM) for 1 h and then treated with LPS. NO concentration (LPS, 25 ng/mL, 24 h) in the medium was determined by the Griess method, and the concentration of IL-6 (LPS, 100 ng/mL, 24 h), TNF-α (LPS, 100 ng/mL, 3 h), and PGE_2 (LPS, 100 ng/mL, 24 h) in the medium was determined by ELISA. The results shown are representative of three independent experiments. $^{###}p < 0.001$ vs untreated controls. $^{**}p < 0.01$, $^{***}p < 0.001$ vs LPS-treated cells.

*3.2.4. Compound **5m** reduced ROS levels in RAW264.7 cells*

Reactive oxygen species (ROS) are chemically reactive chemical species containing oxygen. In a biological system, ROS are formed as a natural byproduct of the normal metabolism of oxygen and have important roles in cell signaling. ROS are also generated as a byproduct of prostaglandin biosynthesis from arachidonic acid by COX-2 [34].

Meanwhile, it is commonly accepted that the state of inflammation induces ROS production and then influences transcription through the regulation of the phosphorylation of transcription factors. Among the transcription factors, nuclear factor-kappa B (NF-κB) is involved in the regulation of pro-inflammatory genes, which represents a key step in the production of pro-inflammatory cytokines, such as tumor necrosis factor-α (TNF-α),

interleukin-6 (IL-6), iNOS, and cyclooxygenase-2 [34,35]. Therefore, we detected and quantified cellular oxidative stress. As shown in Figures 6A and 6B, compound **5m** significantly and dose-dependently reduced ROS production compared with the LPS-treatment group. Notably, at a concentration of 20 μM, compound **5m** significantly decreased ROS production with a potency comparable with that of 20 μM diclofenac. Therefore, we speculated that **5m** inhibited NF-κB activity through the reduction of ROS and the subsequent blocking of the NF-κB transcriptional activity of the pro-inflammatory molecules.

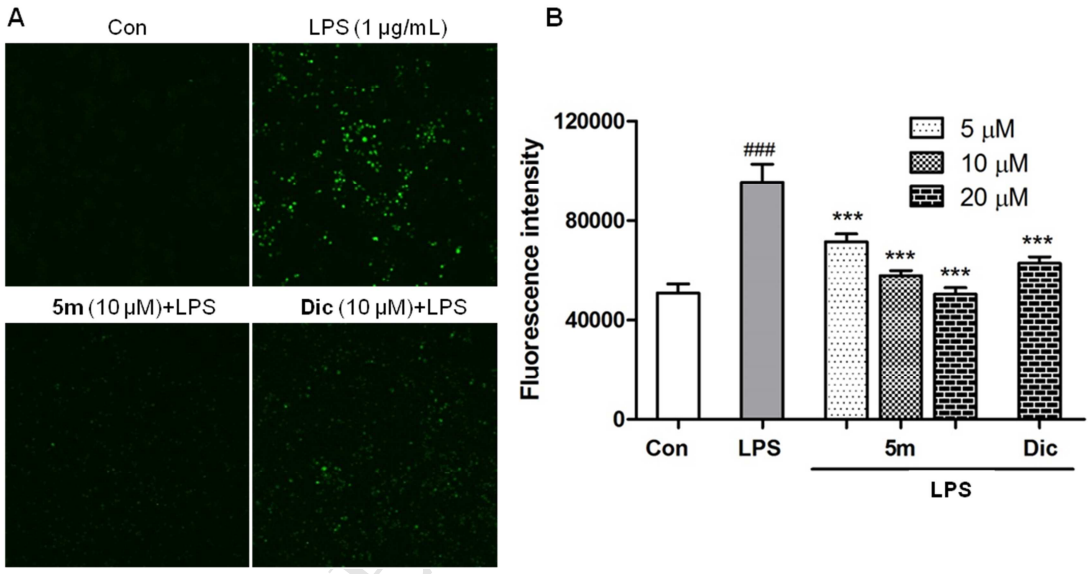

Fig. 6. Reduction of ROS in RAW264.7 cells treated with **5m** and diclofenac (Dic). (**A**) LPS (1 μg/mL) induced intracellular ROS, which is indicated as green fluorescence by the fluorescent probe, DCFH-DA. Through treatment with **5m** or diclofenac (Dic) (10 μM), ROS expression was significantly decreased. (**B**) The fluorescence intensity was quantified by using a fluorescence microplate reader. $^{###}p < 0.001$ vs untreated controls. $^{***}p < 0.001$ vs LPS-treated cells.

*3.2.5. LPS-induced NF-κB signaling was repressed by treatment with **5m***

To investigate further the possible anti-inflammatory mechanism of **5m**, the effect of **5m** on the NF-κB pathway was examined. In the present study, we first used Western blotting to investigate the induction of NF-κB p65 phosphorylation by treatment with **5m** in LPS-activated RAW264.7 cells. Cell extracts were collected after LPS stimulation for 30 min

to detect the early state of NF-κB p65 signaling. As shown in Figure 7B, the levels of phosphorylated NF-κB p65 were clearly increased by LPS treatment, but the treatment of **5m** repressed NF-κB p65 phosphorylation in a dose-dependent manner (Fig. 7B). The phosphorylation of IκB (inhibitor of NF-κB) and IKK (IκB-kinase) is essential for the process of the nuclear translocation and activation of NF-κB. Inflammatory stimuli, such as toxins, pathogens, or oxidative stress, induce the phosphorylation of IKK. After phosphorylation, IKK is as an essential element in the promotion of IκBα phosphorylation, and phosphorylated IκBα is then ubiquitinated and degraded to release active NF-κB. Subsequently, activated NF-κB translocates to the nucleus to bind to DNA and promotes the expression of pro-inflammatory factors [36]. As expected, LPS stimulation markedly increased the level of phosphorylated IKK; however, it was obviously decreased by the treatment of **5m**. In addition, the level of phosphorylated IκBα was also reduced compared with the LPS-treated group (Fig. 7C and 7D). Furthermore, the immunofluorescence assay showed that the LPS-stimulated translocation of NF-κB into the nucleus was reduced by treatment with **5m** at 20 μM (Fig. 7A). These results indicated that **5m** may exert its anti-inflammatory activity through a reduction in ROS level and the suppression of NF-κB activation in RAW264.7 cells (Fig. 9).

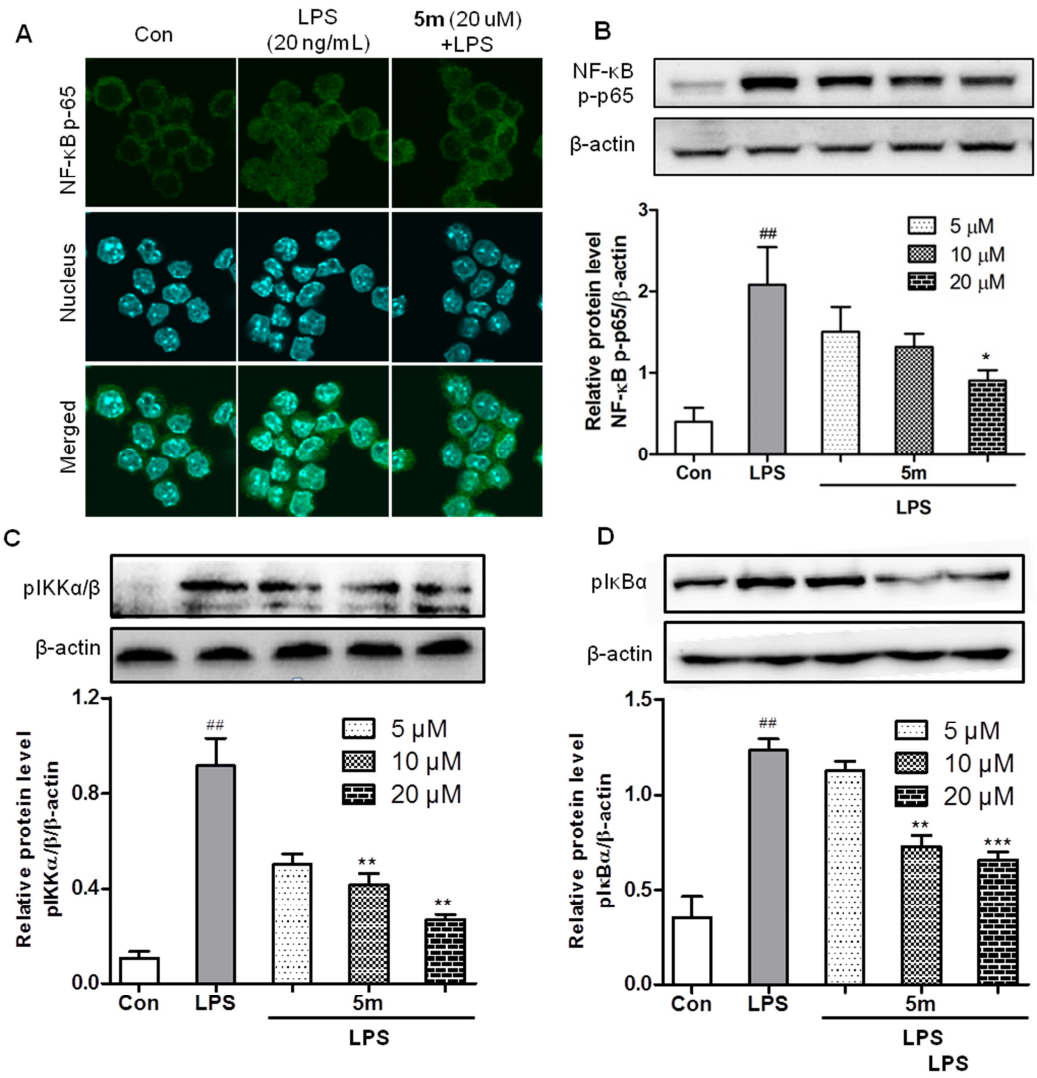

Fig. 7. Effect of compound **5m** on NF-κB activation in RAW264.7 macrophages. (**A**) NF-κB p65 was visualized using confocal microscopy as green fluorescence and the cell nucleus was viewed as cyan fluorescence by DAPI staining. (**B**) Phosphorylation of NF-κB. (**C**) Phosphorylation of IKK. (**D**) Phosphorylation of IκBα. The cells were pretreated with compound **5m** for 1 h and then stimulated with lipopolysaccharide (LPS, 20 ng/mL) for 15 min; β-actin was used as the internal control. The results shown are representative of three independent experiments. $^{\#\#}p < 0.01$ vs untreated controls. $^{*}p < 0.05$, $^{**}p < 0.01$, $^{***}p < 0.001$ vs LPS-treated cells.

3.3. Molecular docking study

The COX-1 and COX-2 inhibitory effects and the in vitro anti-inflammatory activity of **5m** led us to perform molecular docking studies to understand the ligand-protein interactions

in detail. To gain insight into the interaction between **5m** and COX enzymes, a docking simulation was performed using ovine COX-1 (PDB ID: *Ovis aries* 1EQH) and murine COX-2 (PDB ID: *Mus musculus* 4COX). The calculated docking poses of **5m** were compared with that of the indomethacin crystal-like pose with COX-2 [25].

Generally, COX-1 and COX-2 share a 60% homology in amino acid sequence. However, the conformation for the substrate-binding sites and the catalytic regions are slightly different. The comparison of any COX-1 and any COX-2 enzymes demonstrates that COX-2 has a larger and more flexible substrate channel than COX-1, and also that COX-2 has a larger space at the site to which selective inhibitors could bind, which is composed of amino acids Val^{523}, Arg^{513}, and His^{90} (Fig. 8A) [12,25,37]. COX-2 selective inhibitors, such as SC-558, are located deep in the large bioactive cavity and the specific moiety could form hydrogen bonds to Arg^{513} and His^{90}. In contrast, non-selective COX inhibitors, such as indomethacin and ibuprofen, also bind in the long hydrophobic channel, but do not occupy the additional pocket present in COX-2 [25].

In addition, there are two important polar amino acids inside the active site in a bent narrow gap. The amino acids Arg^{120} and Tyr^{355}, which are located deeper in the active site, play an important role in the stabilization of the carboxyl group of classical non-selective NSAIDs in the hydrophobic COX channel. The carboxyl group of the drug forms a hydrogen bond with the guanidium group of Arg^{120} and Tyr^{355} in the binding site (Fig. 8B) [9,12,25]. Notably, compound **5m** showed identical hydrogen bond poses with NSAIDs in COX-1 and COX-2 (Fig. 8C and 8D), which indicated that the carboxylate group of the NSAIDs could be replaced by an aryl-hydrazone moiety. These interactions were almost essential for COX-1/COX-2 inhibitory activity, as exemplified by the binding interaction of indomethacin [25]. Meanwhile, compound **5m** did not form hydrogen bonds with Arg^{513} and His^{90}. This lack of binding may explain the non-significant selectivity of **5m** to COX-2.

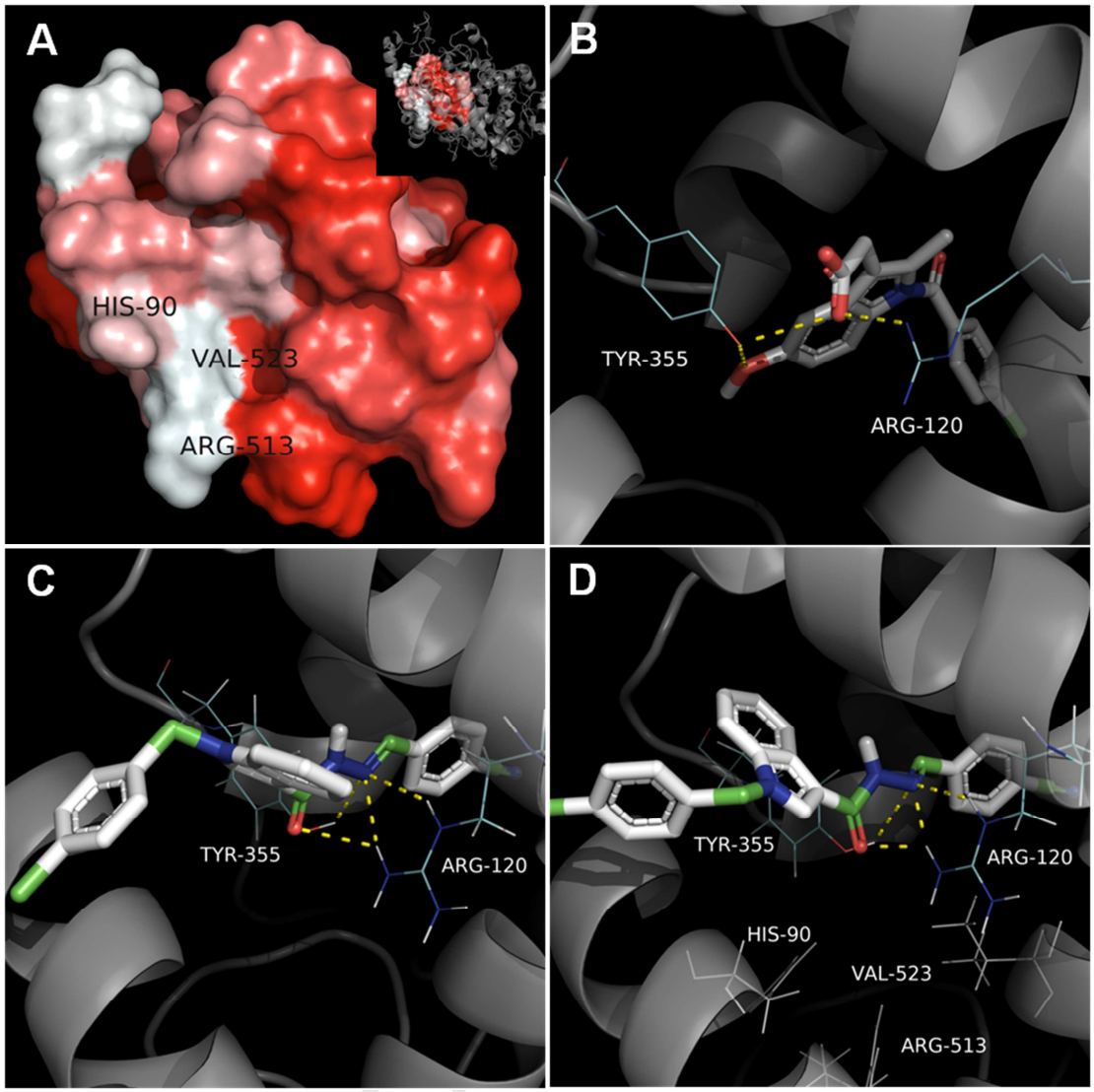

Fig. 8. Docking and crystal structures of ligand/COX binding. (**A**) Zoomed view of the bioactive pocket of the COX-2 (4COX) (the hydrophobic and hydrophilic regions of COX-2 are shown in red and white, respectively). An additional larger space is composed of amino acids of Val^{523}, Arg^{513}, and His^{90}. (**B**) Zoomed view of the crystal structure of the COX-2 bound to indomethacin (4COX). The carboxyl group of indomethacin forms hydrogen bonds with Arg^{120} and Tyr^{355} of COX-2 LBD. (**C**) Zoomed view of the hydrogen bonding interactions between **5m** and the surrounding amino acids, Arg^{120} and Tyr^{355} in COX-1 (1EQH). (**D**) Zoomed view of the hydrogen bonding interactions between **5m** and the surrounding amino acids, Arg^{120} and Tyr^{355} in COX-2 (4COX). 4COX is a murine COX-2 (PDB ID: *Mus musculus* 4COX) and 1EQH is an ovine COX-1 (PDB ID: *Ovis aries* 1EQH).

4. Conclusion

We designed and synthesized two series of new indole substituted derivatives **5a**–**5u** and **6a**–**6b** as COX inhibitors. These derivatives were tested for in vitro COX-1 and COX-2 inhibition. Compound **5m** showed most the potent inhibition of both enzymes with higher selectivity to COX-2, close to that of diclofenac. Compound **5m** was, thus, selected as a balanced COX inhibitor and evaluated for its in vitro anti-inflammatory activity. Compound **5m** exerted anti-inflammatory activity through the suppression of the expression of pro-inflammatory factors, including iNOS, NO, COX-2, PGE_2, TNF-α, and IL-6 in LPS-stimulated murine RAW264.7 macrophages. A reduction in ROS was also observed. Compound **5m** decreased the phosphorylation of IKK, IκBα, and NF-κB. A possible anti-inflammatory mechanism of **5m** was proposed based on the in vitro results. Compound **5m** may first inhibit COX-2, leading to a decrease in ROS production. Decreased ROS production culminates in the suppression of NF-κB activation and endonuclear translocation, thereby attenuating the expression of pro-inflammatory mediators, such as iNOS, COX-2, TNF-α, and IL-6 (Fig. 9). These results may have important implications for the therapeutic potential of **5m**, and compound **5m** may serve as a potential anti-inflammatory lead. Further investigation on the comparison of side effects with NSAIDs, especially non-selective and selective COX inhibitors, may be of value.

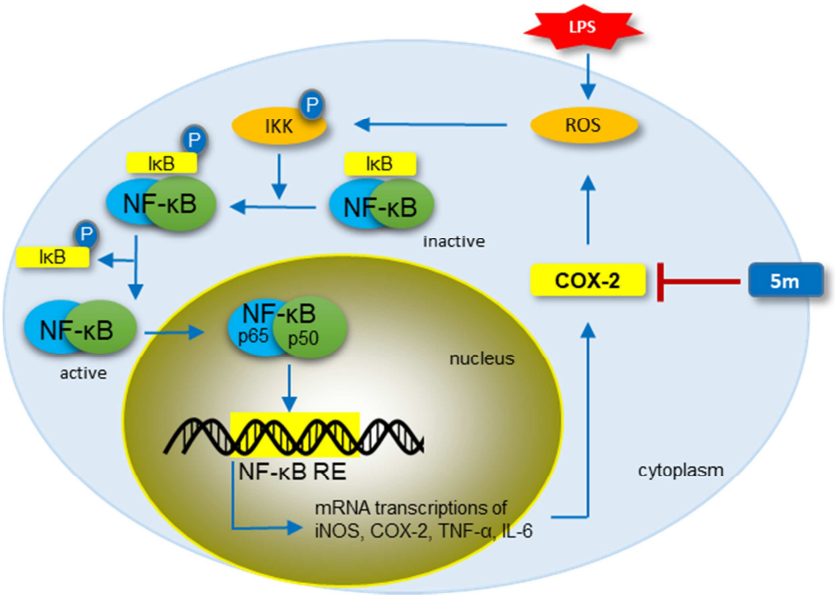

Fig. 9. A diagram of the speculative anti-inflammatory mechanism of the COX inhibitor **5m** in

LPS-induced RAW264.7 cells.

5. Experimental section

5.1. Chemistry

All reagents used were commercially available; some organic solvents were redistilled under a positive pressure, if necessary. Reactions were monitored by thin-layer chromatography (TLC) on glass plates coated with silica gel using a fluorescent indicator (GF254, Merck, Germany). The ^{1}H and ^{13}C NMR spectral data were recorded on Varian Unity 500 MHz and 400 MHz NMR spectrometers, respectively. The high-resolution fast-atom bombardment mass spectrometry (HRFABMS) data were obtained by using an Agilent 1200 UHPLC accurate-mass Q-TOF MS spectrometer. All chemical reagents were purchased from Sigma-Aldrich and Alfa Aesar.

*5.1.1. Synthesis of compounds **5a**–**5u***

General procedure for **2**: A solution of indole-3-carboxylic acid (1.0 mmol-equiv.) and the appropriate anhydrous methyl alcohol (25 mL) were refluxed in the presence of a few drops of sulfuric acid (97%) for 24 h. The progress of the reaction was monitored by TLC (Silica gel $60F_{254}$, Merck, Germany). Precipitated 1*H*-indole-3-carboxylate methyl ester was filtered and recrystallized from an ethanol-water (3:2) mixture.

5.1.1.1. Methyl ^{1}H-indole-3-carboxylate **2**. Pale yellow solid after recrystallization; 77% yield

^{1}H-NMR (500 MHz, DMSO-d_6, δ = ppm) δ 11.94 (s, 1H), 8.09 (s, 1H), 8.02 (d, J = 7.5 Hz, 1H), 7.50 (d, J = 7.6 Hz, 1H), 7.26–7.14 (m, 2H), 3.81 (s, 3H). ^{13}C-NMR (125 MHz, DMSO-d_6, δ = ppm) δ 164.8, 136.4, 132.4, 125.7, 122.4, 121.3, 120.4, 112.4, 106.3, 50.6. HRFABMS *m/z* 176.0673 $[M+H]^+$ (calcd for $C_{10}H_9NO_2$, 176.0706).

General procedure for **4a**–**u**: 1*H*-Indole-3-carboxylate methyl ester **2** (1.0 mmol-equiv.) was refluxed with hydrazine hydrate (12.5 g, 0.25 M) in appropriate ethanol (30 mL) for 2 h. The progress of the reaction was monitored by TLC. After cooling the reaction mixture to room temperature, the mixtures were filtered to give white solid crude products without purification.

Next, indole-hydrazide (**3**, 1.0 mmol) in ethanol (30 mL) was added dropwise into the appropriate aldehyde (1.5 mmol-equiv.) and a few drops of propionic acid; the mixture was stirred and refluxed for 2.5 h. After cooling, the precipitates were filtered and washed several times by methanol to yield the crystal substances **4a**–**u**.

General procedure for **5a**–**u/6a**–**b**: A solution of **4a**–**u** (1 mmol) in DMF (10 mL) was added to the solution of sodium hydride (NaH) (1.5 mmol) in DMF (10 mL) and the reaction mixture was stirred for 1 h at room temperature. Benzyl chloride/benzoyl chloride (1.5 mmol) was added, and the reaction mixture was stirred for 24 h at room temperature. The reaction mixture was poured into ice water, filtered off, and then washed several times with methanol to yield the target compounds **5a**–**u/6a**–**b**.

5.1.1.1. (E)-1-(4-Chlorobenzyl)-N'-(2-methylpropylidene)-1H-indole-3-carbohydrazide **5a**. Pale yellow solid after recrystallization; 35% yield:

^{1}H-NMR (500 MHz, DMSO-d_6, δ = ppm) δ 10.92 (s, 1H), 8.20 (s, 1H), 7.54 (d, J = 7.9 Hz, 1H), 7.41 (m, 2H), 7.28 (d, J = 8.1 Hz, 2H), 7.18 (m, 2H), 7.17 (m, 2H), 5.49 (s, 2H), 2.53 (m, 1H), 1.06 (d, J = 6.5 Hz, 6H). ^{13}C-NMR (125 MHz, DMSO-d_6, δ = ppm) δ 164.1, 155.2, 136.0, 132.3, 129.3, 128.7 (×6), 122.4, 121.0 (×2), 110.6 (×2), 48.7, 30.9, 19.7 (×2). HRFABMS *m/z* 354.1358 $[M+H]^+$ (calcd for $C_{20}H_{20}ClN_3O$, 354.1368).

5.1.1.2. (E)-1-(4-Chlorobenzyl)-N'-(2,2-dimethylpropylidene)-1H-indole-3-carbohydrazide **5b**. Pale yellow solid after recrystallization; 55% yield:

^{1}H-NMR (500 MHz, DMSO-d_6, δ = ppm) δ 10.87 (s, 1H), 8.22 (s, 1H), 7.55 (d, J = 7.8 Hz, 1H), 7.41 (d, J = 8.4 Hz, 2H), 7.29 (d, J = 7.7 Hz, 2H), 7.19 (m, 2H), 7.17 (m, 2H), 5.48 (s, 2H), 1.07 (s, 9H). ^{13}C-NMR (125 MHz, DMSO-d_6, δ = ppm) δ 165.6, 156.1, 135.9, 132.3, 129.3, 128.7 (×6), 122.4, 121.0 (×2), 110.6 (×2), 48.7, 34.4, 19.7 (×3). HRFABMS *m/z* 368.1525 $[M+H]^+$ (calcd for $C_{21}H_{22}ClN_3O$, 368.1524).

5.1.1.3. (E)-1-(4-Chlorobenzyl)-N'-(2-methylbutylidene)-1H-indole-3-carbohydrazide **5c**. Pale yellow solid after recrystallization; 42% yield:

^{1}H-NMR (500 MHz, DMSO-d_6, δ = ppm) δ 10.95 (s, 1H), 8.20 (s, 1H), 7.54 (d, J = 7.9 Hz, 1H), 7.42 (m, 2H), 7.28 (d, J = 8.3 Hz, 2H), 7.20 (m, 2H), 7.17 (m, 2H), 5.50 (s, 2H),

2.31 (m, 1H), 1.50 (m, 1H), 1.40 (m, 1H), 1.05 (d, *J* = 6.2 Hz, 3H), 0.90 (t, *J* = 7.4 Hz, 3H). ^{13}C-NMR (125 MHz, DMSO-d_6, δ= ppm) δ 164.3, 153.9, 136.3, 132.3, 129.3, 128.7 (×6), 122.4, 121.1 (×2), 110.6 (×2), 48.7, 37.6, 27.0, 17.3, 11.4. HRFABMS *m/z* 368.1525 $[M+H]^+$ (calcd for $C_{21}H_{22}ClN_3O$, 368.1524).

5.1.1.4. (E)-1-(4-Chlorobenzyl)-N'-(cyclopropylmethylene)-1H-indole-3-carbohydrazide **5d**. Pale yellow solid after recrystallization; 60% yield:

^{1}H-NMR (500 MHz, DMSO-d_6, δ = ppm) δ 10.91 (s, 1H), 8.15 (s, 1H), 7.49 (d, *J* = 8.0 Hz, 1H), 7.39 (m, 2H), 7.24 (d, *J* = 8.5 Hz, 2H), 7.16 (m, 2H), 7.14 (m, 2H), 5.48 (s, 2H), 1.66 (m, 1H), 0.86 (dd, *J* = 8.1, 2.2 Hz, 2H), 0.63 (dd, *J* = 6.6, 4.1 Hz, 2H). ^{13}C-NMR (125 MHz, DMSO-d_6, δ = ppm) δ 165.3, 154.1, 136.2, 132.2, 129.1 (×2), 128.6 (×4), 122.3, 121.5, 120.9 (×2), 110.5 (×2), 48.7, 13.4, 5.8 (×2). HRFABMS *m/z* 352.1205 $[M+H]^+$ (calcd for $C_{20}H_{18}ClN_3O$, 352.1211).

5.1.1.5. (E)-1-(4-Chlorobenzyl)-N'-(cyclohexylmethylene)-1H-indole-3-carbohydrazide **5e**. Pale yellow solid after recrystallization; 45% yield:

^{1}H-NMR (500 MHz, DMSO-d_6, δ = ppm) δ 10.93 (s, 1H), 8.13 (s, 1H), 7.54 (d, *J* = 7.6 Hz, 1H), 7.41 (d, *J* = 8.2 Hz, 2H), 7.28 (d, *J* = 7.6 Hz, 2H), 7.18 (m, 2H), 7.16 (m, 2H), 5.49 (s, 2H), 2.23 (m, 1H), 1.73 (m, 4H), 164 (m, 1H), 1.29 (m, 1H), 1.24 (m, 4H). ^{13}C-NMR (125 MHz, DMSO-d_6, δ = ppm) δ 164.1, 152.8, 136.2, 132.3, 129.2, 128.6 (×4), 122.3 (×2), 121.5, 121.0 (×2), 110.5 (×2), 48.7, 29.8 (×2), 25.6, 25.1 (×3). HRFABMS *m/z* 394.1668 $[M+H]^+$ (calcd for $C_{23}H_{24}ClN_3O$, 394.1681).

5.1.1.6. (E)-1-(4-Chlorobenzyl)-N'-hexylidene-1H-indole-3-carbohydrazide **5f**. Pale yellow solid after recrystallization; 50% yield:

^{1}H-NMR (500 MHz, DMSO-d_6, δ = ppm) δ 10.96 (s, 1H), 8.19 (s, 1H), 7.52 (d, *J* = 7.9 Hz, 1H), 7.40 (m, 2H), 7.25 (m, 2H), 7.18 (m, 2H), 7.15 (m, 2H), 5.50 (s, 2H), 2.24 (m, 2H), 1.49 (m, 2H), 1.29 (m, 4H), 0.87 (t, *J* = 5.6 Hz, 3H). ^{13}C-NMR (125 MHz, DMSO-d_6, δ = ppm) δ 166.3, 153.8, 136.2 (×2), 132.2, 129.0 (×2), 128.6 (×2), 122.3 (×2), 121.5, 120.9 (×2), 110.5 (×2), 48.7, 31.7, 30.7, 25.7, 21.8, 13.7. HRFABMS *m/z* 382.1695 $[M+H]^+$ (calcd for $C_{22}H_{24}ClN_3O$, 382.1681).

5.1.1.7. (E)-1-(4-Chlorobenzyl)-N'-nonylidene-1H-indole-3-carbohydrazide **5g**. Pale yellow solid after recrystallization; 55% yield:

^{1}H-NMR (500 MHz, DMSO-d_6, δ = ppm) δ 10.95 (s, 1H), 8.17 (s, 1H), 7.50 (d, *J* = 8.0 Hz, 1H), 7.38 (d, *J* = 8.4 Hz, 2H), 7.24 (d, *J* = 8.4 Hz, 2H), 7.16 (m, 2H), 7.15 (m, 2H), 5.48 (s, 2H), 2.23 (dd, *J* = 12.9, 7.3 Hz, 2H), 1.47 (m, 2H), 1.24 (m, 10H), 0.83 (t, *J* = 6.4 Hz, 3H). ^{13}C-NMR (125 MHz, DMSO-d_6, δ = ppm) δ 165.5, 154.5, 136.2 (×2), 132.2, 128.9 (×2), 128.5 (×2), 122.3×2, 121.5, 120.9×2, 110.5 (×2), 48.7, 31.7, 31.1, 28.7, 28.5, 26.0, 23.2, 21.9, 13.8. HRFABMS *m/z* 424.2143 $[M+H]^+$ (calcd for $C_{25}H_{30}ClN_3O$, 424.2150).

5.1.1.8. (E)-1-(4-Chlorobenzyl)-N'-(3-phenylpropylidene)-1H-indole-3-carbohydrazide **5h**. Pale yellow solid after recrystallization; 65% yield:

^{1}H-NMR (500 MHz, DMSO-d_6, δ = ppm) δ 11.04 (s, 1H), 8.17 (s, 1H), 7.59 (s, 1H), 7.49 (d, *J* = 8.0 Hz, 1H), 7.37 (d, *J* = 7.7 Hz, 2H), 7.26 (m, 6H), 7.17 (m, 2H), 7.14 (m, 2H), 5.47 (s, 2H), 2.82 (t, *J* = 7.7 Hz, 2H), 2.57 (dt, *J* = 12.7, 6.3 Hz, 2H). ^{13}C-NMR (125 MHz, DMSO-d_6, δ= ppm) δ 163.8, 153.3, 141.1, 136.2 (×2), 135.9, 132.3, 129.1, 128.7 (×2), 128.4 (×2), 128.3 (×2), 125.9, 122.4 (×2), 121.5, 121.1 (×2), 110.6 (×2), 48.8, 33.6, 32.2. HRFABMS *m/z* 416.1517 $[M+H]^+$ (calcd for $C_{25}H_{22}ClN_3O$, 416.1524).

5.1.1.9. (E)-N'-benzylidene-1-(4-chlorobenzyl)-1H-indole-3-carbohydrazide **5i**. Pale yellow solid after recrystallization; 45% yield:

^{1}H-NMR (500 MHz, DMSO-d_6, δ = ppm) δ 11.48 (s, 1H), 8.36 (s, 1H), 8.25 (s, 1H), 7.68 (s, 1H), 7.58 (d, *J* = 7.9 Hz, 1H), 7.44 (m, 5H), 7.34 (s, 2H), 7.22 (m, 2H), 7.21 (m, 2H), 5.56 (s, 2H). ^{13}C-NMR (125 MHz, DMSO-d_6, δ = ppm) δ 164.4, 154.3, 136.2 (×2), 135.9, 134.6 (×2), 132.3, 129.5, 129.3, 128.8 (×2), 128.7 (×2), 126.7, 122.5 (×2), 121.5, 121.2 (×2), 110.6 (×2), 48.8. HRFABMS *m/z* 388.1198 $[M+H]^+$ (calcd for $C_{23}H_{18}ClN_3O$, 388.1211).

5.1.1.10. (E)-1-(4-Chlorobenzyl)-N'-(4-hydroxybenzylidene)-1H-indole-3-carbohydrazide **5j**. Pale yellow solid after recrystallization; 80% yield:

^{1}H-NMR (500 MHz, DMSO-d_6, δ = ppm) δ 11.70 (s, 1H), 11.26 (s, 1H), 8.23 (s, 1H), 8.20 (s, 1H), 7.66 (d, *J* = 8.6 Hz, 1H), 7.50 (m, 5H), 7.18 (m, 2H), 7.16 (m, 2H), 7.10 (d, *J* =

458 8.7 Hz, 2H), 5.17 (s, 2H). ^{13}C-NMR (125 MHz, DMSO-d_6, δ = ppm) δ 168.9, 159.2, 156.4,
459 135.8, 132.4, 129.4 (×3), 128.4 (×3), 128.2 (×2), 127.7, 122.1 (×2), 121.1, 120.6 (×2), 115.2
460 (×2), 111.8, 68.5. HRFABMS *m/z* 404.1165 $[M+H]^+$ (calcd for $C_{23}H_{18}ClN_3O_2$, 404.1160).

461 *5.1.1.11. (E)-1-(4-Chlorobenzyl)-N'-(4-chlorobenzylidene)-1H-indole-3-carbohydrazide* **5k**.
462 Pale yellow solid after recrystallization; 85% yield:

463 ^{1}H-NMR (500 MHz, DMSO-d_6, δ = ppm) δ 11.46 (s, 1H), 8.30 (s, 1H), 8.22 (s, 1H), 7.67
464 (s, 1H), 7.56 (d, *J* = 8.0 Hz, 1H), 7.49 (d, *J* = 8.3 Hz, 2H), 7.42 (d, *J* = 8.3 Hz, 2H), 7.30 (d, *J*
465 = 7.3 Hz, 2H), 7.21 (m, 2H), 7.18 (m, 2H), 5.53 (s, 2H). ^{13}C-NMR (125 MHz, DMSO-d_6, δ =
466 ppm) δ 166.1, 154.3, 136.1, 135.8, 133.8, 133.5, 132.3, 129.2 (×2), 128.8 (×2), 128.6 (×2),
467 128.2 (×2), 122.5 (×2), 121.4, 121.2 (×2), 110.6 (×2), 48.7. HRFABMS *m/z* 422.0828 $[M+H]^+$
468 (calcd for $C_{23}H_{17}Cl_2N_3O$, 422.0821).

469 *5.1.1.12. (E)-1-(4-Chlorobenzyl)-N'-(4-methoxybenzylidene)-1H-indole-3-carbohydrazide* **5l**.
470 Pale yellow solid after recrystallization; 85% yield:

471 ^{1}H-NMR (500 MHz, DMSO-d_6, δ = ppm) δ 11.31 (s, 1H), 8.24 (s, 2H), 7.60 (s, 1H), 7.57
472 (d, *J* = 7.9 Hz, 1H), 7.45 (m, 2H), 7.33 (m, 2H), 7.22 (m, 2H), 7.20 (m, 2H), 7.01 (d, *J* = 8.3
473 Hz, 2H), 5.54 (s, 2H), 3.81 (s, 3H). ^{13}C-NMR (125 MHz, DMSO-d_6, δ = ppm) δ 163.9, 160.4,
474 154.3, 136.2 (×2), 135.2, 132.4, 129.3, 128.6 (×2), 128.2 (×2), 127.2, 122.4 (×2), 121.5, 121.1
475 (×2), 114.3 (×2), 110.5 (×2), 55.2, 48.7. HRFABMS *m/z* 418.1322 $[M+H]^+$ (calcd for
476 $C_{24}H_{20}ClN_3O_2$, 418.1317).

477 *5.1.1.13. (E)-1-(4-Chlorobenzyl)-N'-(4-cyanobenzylidene)-1H-indole-3-carbohydrazide* **5m**.
478 Pale yellow solid after recrystallization; 58% yield:

479 ^{1}H-NMR (500 MHz, DMSO-d_6, δ = ppm) δ 11.49 (s, 1H), 8.32 (s, 1H), 8.23 (s, 1H), 7.64
480 (m, 3H), 7.57 (d, *J* = 8.0 Hz, 1H), 7.44 (d, *J* = 8.2 Hz, 2H), 7.32 (d, *J* = 7.2 Hz, 2H), 7.22 (m,
481 2H), 7.21 (m, 2H), 5.55 (s, 2H). ^{13}C-NMR (125 MHz, DMSO-d_6, δ = ppm) δ 168.2, 157.4,
482 139.8, 136.8, 136.6, 133.3 (×2), 133.1, 130.0, 129.4 (×4), 129.2, 127.9 (×2), 123.3, 122.1,
483 122.0 (×2), 119.3, 111.9, 111.4, 49.4. HRFABMS *m/z* 413.1168 $[M+H]^+$ (calcd for
484 $C_{24}H_{17}ClN_4O$, 413.1164).

5.1.1.14. (E)-N'-(4-bromobenzylidene)-1-(4-chlorobenzyl)-1H-indole-3-carbohydrazide **5n**. Pale yellow solid after recrystallization; 65% yield:

^{1}H-NMR (500 MHz, DMSO-d_6, δ = ppm) δ 11.66 (s, 1H), 8.35 (s, 1H), 8.23 (s, 1H), 7.90 (m, 1H), 7.86 (s, 2H), 7.58 (d, *J* = 8.2 Hz, 1H), 7.45 (d, *J* = 7.2 Hz, 2H), 7.32 (*J* = 7.7 Hz, 2H), 7.23 (m, 2H), 7.21 (m, 2H), 5.56 (s, 2H). ^{13}C-NMR (125 MHz, DMSO-d_6, δ = ppm) δ 164.8, 155.7, 136.1 (×2), 135.8, 133.9, 132.3 (×2), 131.7, 129.2 (×2), 128.6 (×2), 128.5 (×2), 122.5 (×2), 121.5, 121.2 (×2), 110.6 (×2), 48.7. HRFABMS *m/z* 466.0314 $[M+H]^+$ (calcd for $C_{23}H_{17}BrClN_3O$, 466.0316).

5.1.1.15. (E)-4-((2-(1-(4-Chlorobenzyl)-1H-indole-3-carbonyl)hydrazono)methyl)benzoic acid **5o**. Pale yellow solid after recrystallization; 78% yield:

^{1}H-NMR (500 MHz, DMSO-d_6, δ = ppm) δ 11.61 (s, 1H), 8.36 (s, 1H), 8.25 (s, 1H), 7.82 (s, 1H), 7.58 (d, *J* = 7.9 Hz, 1H), 7.54 (d, *J* = 8.4 Hz, 2H), 7.49 (m, 2H), 7.43 (d, *J* = 8.4 Hz, 1H), 7.32 (d, *J* = 7.8 Hz, 2H), 7.24 (m, 2H), 7.22 (m, 2H), 5.37 (s, 2H). ^{13}C-NMR (125 MHz, DMSO-d_6, δ = ppm) δ 166.3, 165.1, 155.2, 139.2, 136.1, 135.0, 132.3, 129.8 (×2), 129.7 (×2), 129.2, 128.6 (×2), 128.4 (×2), 126.8, 122.5 (×2), 121.4, 121.2 (×2), 110.6, 48.7. HRFABMS *m/z* 432.0966 $[M+H]^+$ (calcd for $C_{24}H_{18}ClN_3O_3$, 432.0964).

5.1.1.16. (E)-1-(4-Chlorobenzyl)-N'-(4-fluorobenzylidene)-1H-indole-3-carbohydrazide **5p**. Pale yellow solid after recrystallization; 85% yield:

^{1}H-NMR (500 MHz, DMSO-d_6, δ = ppm) δ 11.43 (s, 1H), 8.31 (s, 1H), 8.23 (s, 1H), 7.72 (s, 1H), 7.57 (d, *J* = 8.0 Hz, 1H), 7.44 (d, *J* = 8.2 Hz, 2H), 7.30 (m, 2H), 7.27 (d, *J* = 8.7 Hz, 2H), 7.21 (m, 2H), 7.17 (m, 2H), 5.54 (s, 2H). ^{13}C-NMR (125 MHz, DMSO-d_6, δ= ppm) δ 165.6, 161.5, 156.9, 136.1, 132.3, 131.2, 129.2 (×2), 128.8 (×2), 128.7 (×2), 128.6 (×2), 122.4, 121.4, 121.1 (×2), 115.8, 115.6, 110.6 (×2), 48.7. HRFABMS *m/z* 406.1112 $[M+H]^+$ (calcd for $C_{23}H_{17}ClFN_3O_3$, 406.1117).

5.1.1.17. (E)-1-(4-Chlorobenzyl)-N'-(3,5-dichlorobenzylidene)-1H-indole-3-carbohydrazide **5q**. Pale yellow solid after recrystallization; 86% yield:

^{1}H-NMR (500 MHz, DMSO-d_6, δ = ppm) δ 11.71 (s, 1H), 8.37 (s, 1H), 8.21 (s, 1H), 7.74

(s, 2H), 7.58 (d, *J* = 7.8 Hz, 1H), 7.42 (d, *J* = 8.3 Hz, 2H), 7.31 (d, *J* = 7.7 Hz, 2H), 7.22 (m, 2H), 7.20 (m, 2H), 5.55 (s, 2H). ^{13}C-NMR (125 MHz, DMSO-d_6, δ = ppm) δ 164.5, 155.2, 136.2 (×2), 134.5 (×2), 129.0 (×2), 128.9 (×2), 128.6 (×2), 128.4, 124.9 (×2), 122.5 (×2), 121.8, 121.2 (×2), 110.6 (×2), 48.7. HRFABMS *m/z* 456.0426 $[M+H]^+$ (calcd for $C_{23}H_{16}Cl_3N_3O$, 456.0286).

5.1.1.18. (E)-1-(4-Chlorobenzyl)-N'-(3,5-dibromobenzylidene)-1H-indole-3-carbohydrazide **5r**. Pale yellow solid after recrystallization; 75% yield:

^{1}H-NMR (500 MHz, DMSO-d_6, δ = ppm) δ 11.71 (s, 1H), 8.36 (s, 1H), 8.21 (s, 1H), 7.88 (s, 2H), 7.57 (d, *J* = 7.8 Hz, 1H), 7.42 (d, *J* = 8.3 Hz, 2H), 7.31 (d, *J* = 7.4 Hz, 2H), 7.22 (m, 2H), 7.20 (m, 2H), 5.54 (s, 2H). ^{13}C-NMR (125 MHz, DMSO-d_6, δ = ppm) δ 162.8, 157.8, 140.8, 138.8, 136.2, 133.6, 132.3, 129.0 (×3), 128.6 (×3), 128.1 (×2), 122.8 (×2), 122.5, 121.2 (×2), 110.6 (×2), 48.7. HRFABMS *m/z* 543.9271 $[M+H]^+$ (calcd for $C_{23}H_{16}Br_2ClN_3O$, 543.9276).

5.1.1. 19.
(E)-N'-(3-chloro-5-methoxybenzylidene)-1-(4-chlorobenzyl)-1H-indole-3-Carbohydrazide **5s**. Pale yellow solid after recrystallization; 75% yield:

^{1}H-NMR (500 MHz, DMSO-d_6, δ = ppm) δ 11.45 (s, 1H), 8.30 (s, 1H), 8.23 (s, 1H), 7.94 (d, *J* = 10.2 Hz, 1H), 7.65 (s, 1H), 7.56 (d, *J* = 7.8 Hz, 1H), 7.42 (d, *J* = 8.3 Hz, 2H), 7.32 (s, 2H), 7.21 (m, 2H), 7.19 (m, 2H), 5.53 (s, 2H), 3.90 (s, 3H). ^{13}C-NMR (125 MHz, DMSO-d_6, δ = ppm) δ 166.0, 156.2, 136.2 (×2), 132.3, 130.6, 129.1 (×2), 128.7, 128.6 (×4), 127.6, 122.4 (×2), 121.4, 121.1 (×2), 112.7, 111.1, 110.6, 56.4, 48.7. HRFABMS *m/z* 496.0259 $[M+H]^+$ (calcd for $C_{24}H_{19}BrClN_3O_2$, 496.0276).

5.1.1.20.
(E)-1-(4-Chlorobenzyl)-N'-((4-methylthiazol-5-yl)methylene)-1H-indole-3-carbohydrazide **5t**. Pale yellow solid after recrystallization; 88% yield:

^{1}H-NMR (500 MHz, DMSO-d_6, δ = ppm) δ 11.49 (s, 1H), 9.00 (s, 1H), 8.59 (s, 1H), 8.26 (s, 1H), 8.20 (s, 1H), 7.55 (d, *J* = 7.8 Hz, 1H), 7.40 (d, *J* = 8.2 Hz, 2H), 7.29 (s, 2H), 7.19 (m, 2H), 5.49 (s, 2H), 2.45 (s, 3H). ^{13}C-NMR (125 MHz, DMSO-d_6, δ = ppm) δ 164.5, 154.1,

153.0, 136.2, 132.4, 129.3, 128.8 (×4), 128.1 (×2), 122.6 (×2), 121.4, 121.3 (×2), 110.7 (×2), 48.8, 15.3. HRFABMS *m/z* 409.0873 $[M+H]^+$ (calcd for $C_{21}H_{17}ClN_4OS$, 409.0884).

5.1.1.21. (E)-1-(4-Chlorobenzyl)-N'-(furan-2-ylmethylene)-1H-indole-3-carbohydrazide **5u**. Pale yellow solid after recrystallization; 67% yield:

^{1}H-NMR (500 MHz, DMSO-d_6, δ = ppm) δ 11.50 (s, 1H), 8.36 (s, 1H), 8.25 (s, 1H), 7.55 (d, *J* = 7.7 Hz, 1H), 7.42 (d, *J* = 8.2 Hz, 2H), 7.31 (d, *J* = 7.1 Hz, 2H), 7.21 (m, 2H), 7.20 (m, 2H), 6.86 (d, *J* = 3.0 Hz, 1H), 6.63 (dd, *J* = 3.1, 1.6 Hz, 1H), 5.53 (s, 2H). ^{13}C-NMR (125 MHz, DMSO-d_6, δ = ppm) δ 166.8, 149.8, 144.5, 136.1 (×2), 135.8, 132.3, 129.2 (×2), 128.6 (×4), 122.5 (×2), 121.5, 121.2 (×2), 112.0, 110.6, 48.8. HRFABMS *m/z* 378.0840 $[M+H]^+$ (calcd for $C_{21}H_{16}ClN_3O_2$, 378.0858).

5.1.1.22. (E)-1-(4-Chlorobenzoyl)-N'-(4-cyanobenzylidene)-1H-indole-3-carbohydrazide **6a**. Pale yellow solid after recrystallization; 88% yield:

^{1}H-NMR (500 MHz, DMSO-d_6, δ = ppm) δ 11.84 (s, 1H), 8.32 (s, 1H), 8.26 (s, 1H), 7.89 (s, 1H), 7.87 (m, 2H), 7.85 (m, 2H), 7.70 (m, 2H), 7.66 (s, 1H), 7.41 (m, 2H), 7.39 (m, 2H). ^{13}C-NMR (125 MHz, DMSO-d_6, δ= ppm) δ 167.7, 163.5, 159.6, 132.5 (×3), 131.3, 128.9 (×6), 127.4, 125.4 (×2), 124.7 (×2), 122.0, 118.5, 115.6 (×2), 111.7 (×2). HRFABMS *m/z* 427.0961 $[M+H]^+$ (calcd for $C_{24}H_{15}ClN_4O_2$, 427.0956).

5.1.1.23. (E)-1-(4-Bromobenzoyl)-N'-(4-cyanobenzylidene)-1H-indole-3-carbohydrazide **6b**. Pale yellow solid after recrystallization; 85% yield:

^{1}H-NMR (500 MHz, DMSO-d_6, δ = ppm) δ 11.88 (s, 1H), 8.36 (s, 1H), 8.29 (s, 1H), 7.90 (s, 1H), 7.88 (m, 2H), 7.87 (m, 2H), 7.83 (m, 2H), 7.72 (s, 1H), 7.46 (m, 2H), 7.43 (m, 2H). ^{13}C-NMR (125 MHz, DMSO-d_6, δ = ppm) δ 168.4, 160.2, 157.4, 145.3, 142.9, 139.3, 133.3 (×2), 132.6 (×5), 132.1, 128.0, 126.1, 125.4 (×2), 122.4, 119.2, 116.3 (×2), 112.4 (×2). HRFABMS *m/z* 471.0441 $[M+H]^+$ (calcd for $C_{24}H_{15}BrN_4O_2$, 471.0451).

5.2. Biological evaluation

5.2.1. In vitro cytotoxicity

5.2.1.1. Cell culture

RAW264.7 murine macrophages were purchased from the Korean Cell Line Bank (KCLB®, Seoul, Korea) and rat liver Ac2F cells and mouse fibroblast cells (L929) were obtained from the American Type Culture Collection (ATCC, Rockville, MD, USA). Cells were cultured at 37°C in a 5% CO_2 humidified incubator and maintained in high glucose Dulbecco's Modified Eagle Medium (DMEM, Nissui, Tokyo, Japan) supplemented with 100 mg/mL streptomycin, 2.5 mg/L amphotericin B, and 10% heat-inactivated fetal bovine serum (FBS).

5.2.1.2. In vitro cytotoxicity assay

Suspensions of tested cell lines (1.0×10^4 cells/well) were seeded in a 96-well culture plates, cultured for 12 h, then treated with various diluted concentrations of **5m** for 24 h. The control cells were treated with culture medium alone. The test compounds were evaluated at three dilutions and the highest concentration was 50 μM. Cell viabilities were evaluated by using water soluble tetrazolium (WST) reagent (EZ-CyTox, Daeil Lab Service Co., Ltd., Seoul, Korea), which was added to each well (10 μL) and incubated at 37°C for 1 h. The absorbance at 450 nm was read by using an iMark Microplate Absorbance Reader (Bio-Rad Laboratories, Hercules, CA, USA). In all experiments, cells in the exponential phase were used.

5.2.1. 3. Cyclooxygenase (COX) inhibition assays

The assay was performed by using a COX fluorescent inhibitor screening assay kit (Cayman Chemical, MI, USA) in accordance with the manufacturer's protocol, COX-1 (ovine) and COX-2 (human recombinant) were utilized to catalyze arachidonic acid into PGG_2, which is reacted with ADHP (10-acetyl-3,7-dihydroxyphenoxazine) to produce the highly fluorescent compound resorufin. Resorufin fluorescence can be analyzed using an excitation wavelength of 510 nm and an emission wavelength of 580 nm. In brief, 150 μL of assay buffer, 10 μL heme, 10 μL enzyme (COX-1 or COX-2), and 10 μL vehicle were mixed in a well to serve as 100% initial activity wells; 160 μL of assay buffer, 10 μL heme and 10 μL vehicle were mixed in a well and served as background wells; 150 μL of assay buffer, 10 μL heme, and 10 μL enzyme (COX-1 or COX-2) and 10 μL compounds were mixed in a well and

served as inhibitor wells. The plate was incubated for 5 min at room temperature, and then 10 μL of ADHP was added to each well. To initiate the reaction, 10 μL of arachidonic acid solution was quickly added to each well, incubated for 2 min at room temperature, and then the fluorescence spectrum was measured by using an excitation wavelength of 510 nm and an emission wavelength of 580 nm by TriStar LB 941 Multimode Microplate Reader (Bad Wildbad, Germany).

5.2.1.4. Production of NO, TNF-α, IL-6, and PGE_2

RAW264.7 macrophages (cal. 1×10^4 cells/well) were seeded in a 96-well culture plate and cultured for 12 h. The cells were pre-treated with various concentrations of drug for 1 h and then co-incubated with 25 ng/mL LPS for 24 h. The NO concentrations in medium were determined by using the Griess assay. Griess reagent (80 μL) was added to the medium supernatants (80 μL) and then incubated at 37°C for 15 min in the dark. The absorbance at 520 nm was measured by using an iMark Microplate Absorbance Reader (Bio-Rad Laboratories, Hercules, CA, USA). NO concentrations were calculated by using 0–100 μM sodium nitrite standards. TNF-α and IL-6 expression in culture medium was quantified by using a sandwich-type ELISA kit (Biolegend, San Diego, CA, USA) and the absorbance at 450 nm was measured. The production of prostaglandin E_2 (PGE_2) in medium was determined by using the PGE_2 express ELISA kit (Cayman Chemical, MI, USA) in accordance with the protocol and the absorbance at 415 nm was measured.

5.2.1.5. Reactive oxygen species (ROS) measurement

RAW264.7 macrophages were grown on a confocal dish and treated with the test compound treatment for 1 h. LPS solution was added into the dish at a final concentration of 1 μg/mL and continually cultured for 24 h. The medium was removed and washed with PBS; DCFH-DA diluted in FBS-free medium to a final concentration of 100 μM was added and cultured at 37°C for 30 min. The medium was removed and the cells were washed once with PBS. The fluorescence was viewed using a confocal microscope (FluoView FV10i; Olympus, Australia) with an excitation wavelength of 485 nm and an emission wavelength of 520 nm.

The quantification of cellular oxidative stress was performed by using a slightly

627 modified previously reported method [38]. RAW264.7 macrophages (cal. 1×10^4 cells/well)
628 were seeded into black 96-well cell culture plates and cultured for 12 h. The cells were
629 pre-treated with test compound for 1 h and then co-incubated with 1 μg/mL LPS for 24 h. The
630 medium was removed and washed with PBS; 100 μL DCFH-DA diluted in FBS-free medium
631 to a final concentration of 100 μM was added and cultured at 37°C for 30 min. The medium
632 was removed, 100 μL PBS was added to each well, and the fluorescence was detected at an
633 excitation wavelength of 485 nm and an emission wavelength of 520 nm by TriStar LB 941
634 Multimode Microplate Reader (Bad Wildbad, Germany).
635
636 *5.2.1.6. Immunofluorescence staining of NF-κB p65 in RAW264.7 cells*
637 The cells were grown on a confocal dish and treated with the test compounds for 24 h.
638 Subsequently, the cells were fixed in 10% formalin solution for 15 min, washed three times
639 with PBS, treated with 0.5% (v/v) Triton X-100/PBS for 15 min, washed three times with
640 PBS again, and then blocked at room temperature for 30 min in 10% FBS/PBS. The cells
641 were then incubated with rabbit anti-NFκB-p65 antibody (Cell Signaling Technology, USA)
642 at 4°C overnight, washed three times with PBS, incubated for 30 min at room temperature
643 with secondary antibody anti-rabbit Alexa 488 (Cell Signaling Technology, USA) as a
644 molecular probe, washed three times with PBS again, and then incubated with DAPI (5
645 μg/mL) at room temperature for 20 min. The localization of NFκB-p65 was observed by
646 using a confocal microscope (FluoView FV10i, Olympus, Australia) with an excitation
647 wavelength of 499 nm and an emission wavelength of 520 nm.
648
649 *5.2.1.7. Western blotting*
650 RAW264.7 cells were harvested and suspended in lysis buffer containing protease and
651 phosphatase inhibitor cocktails. The protein concentration was determined by using a BCA
652 protein assay (Thermo Scientific, Rockford, IL, USA). Equal amounts of proteins were
653 resolved by 10% SDS-polyacrylamide gel electrophoresis and electrophoretically transferred
654 to polyvinylidene difluoride (PVDF) membranes. Non-specific binding to the membranes was
655 blocked by incubation of the membrane in Tris-buffered saline containing 0.1% Tween 20
656 (TBS-T) and 5% skimmed milk for 1 h at room temperature, and then incubated with specific

primary antibodies (Cell Signaling Technology, Danvers, MA, USA) overnight at 4°C. Anti-rabbit IgG-HRP was used as the secondary antibody. The signals were developed by using the ChemiDoc™Touch Imaging System (Bio-Rad Laboratories, Hercules, CA, USA).

5.3. Molecular modeling

Docking calculations were performed by using AutoDock Vina 1.1.2 software. The default settings and scoring function of Vina were applied. To prepare the ligands, Chem3D Ultra 8.0 software was used to convert the 2D structures of the candidates into 3D structural data with the minimized energy. The protein coordinates were downloaded from the Protein Data Bank (accession code 1EQH/4COX). Chain A was prepared for docking within the molecular modeling software package, Chimera 1.5.3, by removal of the additional chains and all ligands and water molecules, as well as by calculating the protonation state of the protein. The addition of polar hydrogen and setting of grid box parameters was performed by using MGLTools 1.5.4 and the exhaustiveness parameter was set to 8. PyMol v1.5 was used for analysis and visual investigation of the ligand-protein interactions of the docking poses.

Acknowledgments

This research is a part of the project entitled “Omics based fishery disease control, technology development, and industrialization” funded by the Korean Ministry of Oceans and Fisheries. M. Su was supported by the PNU postdoc program (2018), and Z. Ju was partially supported by China Scholarship Council (No. 201608260116).

References

[1] J. Crofford L, Use of NSAIDs in treating patients with arthritis, Arthritis. Res. Ther. 15 (2013) S2.

[2] C.M. Moldovan, O. Oniga, A. Pârvu, B. Tiperciuc, P. Verite, A. Pîrnău, O. Crişan, M. Bojiţă, R. Pop, Synthesis and anti-inflammatory evaluation of some new acyl-hydrazones bearing 2-aryl-thiazole, Eur. J. Med. Chem. 46 (2011) 526-534.

[3] A.K. Nussler, T.R. Billiar, Inflammation, immunoregulation, and inducible nitric oxide synthase, J. Leukoc. Boil. 54 (1993) 171-178.

[4] H. Ohshima, H. Bartsch, Chronic infections and inflammatory processes as cancer risk factors: possible role of nitric oxide in carcinogenesis, Mutat. Res. 305 (1994) 253-264.

[5] M.M. Ahlström, M. Ridderström, I. Zamora, K. Luthman, CYP2C9 structure-metabolism relationships: Optimizing the metabolic stability of COX-2 inhibitors, J. Med. Chem. 50 (2007) 4444-4452.

[6] A.K. Gupta, R.A. Gupta, L.K. Soni, S.G. Kaskhedikar, Exploration of physicochemical properties and molecular modelling studies of 2-sulfonyl-phenyl-3-phenyl-indole analogs as cyclooxygenase-2 inhibitors, Eur. J. Med. Chem. 43 (2008) 1297-1303.

[7] A. Tanaka, H. Araki, Y. Komoike, S. Hase, K. Takeuchi, Inhibition of both COX-1 and COX-2 is required for development of gastric damage in response to nonsteroidal antiinflammatory drugs, J. Physiol. Paris. 95 (2001) 21-27.

[8] J.L. Wallace, W. McKnight, B.K. Reuter, N. Vergnolle, NSAID-induced gastric damage in rats: requirement for inhibition of both cyclooxygenase 1 and 2, Gastroenterology, 119 (2000) 706-714.

[9] P.F. Lamie, W.A.M. Ali, V. Bazgier, L. Rarova, Novel N-substituted indole Schiff bases as dual inhibitors of cyclooxygenase-2 and 5-lipoxygenase enzymes: Synthesis, biological activities in vitro and docking study, Eur. J. Med. Chem. 123 (2016) 803-813.

[10] E.A. Meade, W.L. Smith, D.L. DeWitt, Differential inhibition of prostaglandin endoperoxide synthase (cyclooxygenase) isozymes by aspirin and other Non-steroidal anti-inflammatory drug, J. Biol. Chem. 268 (1993) 6610-6614.

[11] C. Charlier, C. Michaux, Dual inhibition of cyclooxygenase-2 (COX-2) and 5-lipoxygenase (5-LOX) as a new strategy to provide safer non-steroidal anti-inflammatory drugs, Eur. J. Med. Chem. 38 (2003) 645-659.

[12] I. Morita, Distinct functions of COX-1 and COX-2, Prostaglandins. Other. Lipid. Mediat. 68 (2002) 165-175.

[13] A. Schäfer, Z. Chovanová, J. Muchová, K. Sumegová, A. Liptáková, Z. Ďuračková, P. Högger, Inhibition of COX-1 and COX-2 activity by plasma of human volunteers after ingestion of French maritime pine bark extract (Pycnogenol), Biomed. Pharmacother. 60 (2006) 5-9.

[14] H.P. Kim, K.H. Son, H.W. Chang, S.S. Kang, Anti-inflammatory plant flavonoids and cellular action mechanisms, J. Pharmacol. Sci. 96 (2004) 229-45.

[15] F. Krötz, Schiele T.M, V. Klauss, H.Y. Sohn, Selective COX-2 inhibitors and risk of myocardial infarction, J. Vasc. Res. 42 (2005) 312-324.

[16] J.L. Li, S.C. Han, E.S. Yoo, S. Shin, J. Hong, Z. Cui, H. Li, J.H. Jung, Anti-inflammatory amino acid derivatives from the ascidian *Herdmania momus*, J. Nat. Prod. 74 (2011) 1792-1797.

[17] J.L. Li, B. Xiao, M.H. Park, E.S. Yoo, S. Shin , J.K. Hong, H.Y. Chung, H.S. Kim, J.H. Jung, PPAR-γ agonistic metabolites from the ascidian *Herdmania momus*, J. Nat. Prod. 75 (2012) 2082-2087.

[18] J. Kaur, A. Bhardwaj, Z.J. Huang, E.E. Knaus, N-1 and C-3 substituted indole Schiff bases as selective COX-2 inhibitors: synthesis and biological evaluation, Bioorg. Med. Chem. Lett. 22 (2012) 2154-2159.

[19] M.A.A. Radwan, E.A. Ragab, N.M. Sabry, S.M.E. Shenawy, Synthesis and biological evaluation of new 3-substituted indole derivatives as potential anti-inflammatory and analgesic agents, Bioorg. Med. Chem. 15 (2007) 3832-3841.

[20] U. Salgın-Gökşen, N. Gökhan-Kelekçi, Ö. Göktaş, Y. Köysal, E. Kılıç, S. Isık, G. Aktay, M. Özalp, 1-Acylthiosemicarbazides, 1, 2, 4-triazole-5(4H)-thiones, 1, 3, 4-thiadiazoles and hydrazones containing 5-methyl-2-benzoxazolinones: synthesis, analgesic-anti-inflammatory and antimicrobial activities, Bioorg. Med. Chem. 15 (2007) 5738-5751.

[21] A.R. Todeschini, A.L.P. de Miranda, K.C.M. da Silva, S.C. Parrini, E.J. Barreiro, Synthesis and evaluation of analgesic, anti-inflammatory and antiplatelet properties of new 2-pyridylarylhydrazone derivatives, Eur. J. Med. Chem. 33 (1998) 189-199.

[22] M.A. Gaston, L.R.S. Dias, A.C.C. Freitas, A.L.P. Miranda, E.J. Barreiro, Synthesis and analgesic properties of new 4-arylhydrazone 1-H pyrazole [3,4-b] pyridine derivatives, Pharm. Acta. Helv. 71 (1996) 213-219.

[23] A. Almasirad, M. Tajik, D. Bakhtiari, A. Shafiee, M. Abobllahi, M.J. Zamani, R. Khorasani, H. Esmaily, Synthesis and analgesic activity of N-arylhydrazone derivatives of mefenamic acid, J. Pharm. Pharm. Sci. 8 (2005) 419-425.

[24] G. Murineddu, G. Loriga, E. Gavini, A.T. Peana, A.C. Mulè, G.A. Pinna, Synthesis and analgesic-anti-inflammatory activities of novel acyl-arylhydrazones with a 5-phenyl-4-R-3-pyrrolyl-acyl moiety, Arch. Pharm. 34 (2001) 393-398.

[25] R.G. Kurumbail, A.M. Stevens, J.K. Gierse, J.J. McDonald, R.A. Stegeman, J.Y. Pak, D. Gildehaus, J.M. Miyashiro, T.D. Penning, K. Seibert, P.C. Isakson, W. C. Stallings, Structural basis for selective inhibition of cyclooxygenase-2 by anti-inflammatory agents, Nature 384 (1996) 644.

[26] M.S. Alam, D.U. Lee, Synthesis, biological evaluation, drug-likeness, and in silico screening of novel benzylidene-hydrazone analogues as small molecule anticancer agents, Arch. Pharm. Res. 39 (2016) 191-201.

[27] B. Liu, R. Li, Y.A. Li, S.Y. Li, J. Yu, B.F. Zhao, A.C. Liao, Y. Wang, Z.W. Wang, A.D. Lu, Y.X. Liu, Q.M. Wang, Discovery of Pimprinine Alkaloids as Novel Agents against a Plant Virus, J. Agric. Food. Chem. 67 (2019) 1795-1806.

[28] R.P. Herrera, D. Roca-López, G. Navarro-Moros, Uncatalyzed Three-Component Synthesis of α-Hydrazido Phosphonates, European. J. Org. Chem. 2010 (2010) 1450-1454.

[29] P. Kovaříková, K. Vávrová, K. Tomalová, M. Schöngut, K. Hrušková, P. Hašková, J. Klimeš, HPLC-DAD and MS/MS analysis of novel drug candidates from the group of aromatic hydrazones revealing the presence of geometric isomers, J. Pharm. Biomed. Anal. 48 (2008) 295-302.

[30] C. Hawkey, A. Kahan, K. Steinbrück, C. Alegre, E. Baumelou, B. Begaud, J. Dequeker, H. Isomäki, G. Littlejohn, J. M.S. Papazoglou, Gastrointestinal tolerability of meloxicam compared to diclofenac in osteoarthritis patients. International MELISSA Study Group. Meloxicam Large-scale International Study Safety Assessment, Br. J. Rheumatol. 37 (1998)

767 937-945.
768 [31] R.F. Willkens, Worldwide clinical safety experience with diclofenac, Semin. Arthritis.
769 Rheum. 15 (1985) 105-110.
770 [32] M.J.S. Langman, J. Weil, P. Wainwright, D.H. Lawson, M.D. Rawlins, R.F.A. Logan, M.
771 Murphy, M.P. Vessey, D.G. Colin-Jones, Risks of bleeding peptic ulcer associated with
772 individual non-steroidal anti-inflammatory drugs, Lancet. 343(1994) 1075-1078.
773 [33] D.M. Mosser, J.P. Edwards, Exploring the full spectrum of macrophage activation, Nat.
774 Rev. Immunol. 8 (2008) 958.
775 [34] I. Minatel, F. Francisqueti, C. Corrêa, G. Lima, Antioxidant activity of γ-oryzanol: A
776 complex network of interactions, Int. J. Mol. Sci. 17 (2016) 1107.
777 [35] H. Ozturk, A. Gezici, H. Ozturk, The effect of celecoxib, a selective COX-2 inhibitor, on
778 liver ischemia/reperfusion-induced oxidative stress in rats, Hepatol. Res. 34 (2006) 76-83.
779 [36] M. Karin, Y. Ben-Neriah, Phosphorylation meets ubiquitination: the control of NF-κB
780 activity, Annu. Rev. Immunol. 18 (2000) 621-663.
781 [37] R. Finkel, M.A. Clark, L.X. Cubeddu, Pharmacology. (2009).
782 [38] H. Wang, J.A. Joseph, Quantifying cellular oxidative stress by dichlorofluorescein assay
783 using microplate reader, Free. Radic. Biol. Med. 27 (1999) 612-616.
784
785

Highlights:

- New balanced cyclooxygenase (COX-1 and COX-2) inhibitors were designed based on anti-inflammatory ascidian metabolites.
- COX-1 and COX-2 inhibitory activity of these analogues was evaluated *in vitro*.
- Compound **5m** showed substantial *in vitro* anti-inflammatory activity *via* inhibition of the NF-κB (nuclear factor-kappa B) pathway.